Atmósfera(1997), 11, pp. 223-237

Stratiform rainfall rates from the water flux balance equation and cloud model

G. W. REUTER and L. XIN

Department of Earth and Atmospheric Sciences University of Alberta, Edmonton, Canada

(Manuscript received June 5, 1997; accepted in final form April 14, 1998)

RESUMEN

La tasa de precipitación estratiforme promediada según el área puede ser estimada por igualación del flujo descendente de la lluvia con el flujo hacia arriba del vapor. Este estudio evalúa la utilidad de este enfoque por comparación de la tasa de precipitación estimada con la calculada, usando un modelo de nubes no hidrostático dependiente del tiempo. La comparación con los resultados del modelo nuboso revela cuan sensitivas las tasas de lluvia del flujo equilibrado acuoso son a la magnitud y profundidad de la convergencia del bajo nivel.

Se encuentra que el modelo nuboso numérico sobreestimó las observaciones de lluvia para el caso de un estudio en Alberta Central en el cual las condiciones inicales y de frontera del campo de convergencia fueron adoptadas a partir de observaciones de radar Doppler. La ecuación de balance del flujo acuoso y las simulaciones nubosas coincidieron en que la tasa de precipitación se volvió más fuerte cuando, ya sea que la magnitud de la convergencia superficial, o la de la profundidad de la misma, fueron aumentadas.

Sin embargo, la ecuación de balance de flujo acuoso consistentemente subestimó las tasas de lluvia del modelo. También, las estimaciones de la precipitación a partir de la ecuación de balance de flujo acuoso no fueron sensibles a la divergencia en las alturas, en tanto que la precipitación del modelo dependía de la distribución de divergencia en los niveles superiores. La conclusión básica que se infiere es que la ecuación de balance del flujo acuoso es fácil de usar, pero puede suministrar sólo una estimación burda de la precipitación con una tendencia a subestimarla.

ABSTRACT

The area-averaged stratiform precipitation rate can be estimated by equating the downward flux of precipitation with the upward flux of vapour. This study evaluates the usefulness of this approach by comparing the estimated rainfall rate with that computed using a time-dependent non-hydrostatic cloud model. Comparison with the cloud model results reveals how sensitive the water flux balance rainfall rates are to the magnitude and depth of the low-level convergence.

It is found that the numerical cloud model overestimated rainfall observations for a case study of central Alberta for which the initial and boundary conditions of the convergence field were adopted from Doppler radar observations. The water flux balance equation and the cloud simulations agreed in that the rainfall rate became stronger when either the magnitude of the surface convergence or the convergence depth was increased.

However, the water flux balance equation consistently underestimated the model rainfall rates. Also, rainfall estimates from water flux balance equation were not sensitive to the divergence aloft, whereas the model rainfall was dependent on the distribution of upper-level divergence. The basic conclusion to be drawn is that the water flux balance equation is easy to use, but can provide only a crude estimate of rainfall with a bias to underestimate.

1. Introduction

It has long been recognized that local rainfall is closely related to convergence in the boundary layer wind field (Hudson, 1971; Ulanski and Garstang, 1978; Wilson and Schreiber, 1986). Observations suggest that low-level convergence greatly supports long-lasting rain events both in the tropics (Ogura *et al.*, 1979; McBride and Gray, 1980; Tollerud and Esbensen, 1985) and in the mid-latitudes (Maddox, 1983; Srivastava *et al.*, 1986). Numerical simulations using cloud models confirmed these findings (Soong and Ogura, 1973; Lipps and Hemler, 1986; Crook and Moncrieff, 1988; Tao and Simpson, 1989).

This paper deals with the issue of whether estimates of the low-level convergence profile can be used to estimate the rate of precipitation falling from stratiform clouds. Specifically, we examine the accuracy and sensitivity of the water flux balance equation that equates the precipitation rate with the moisture convergence. The water flux balance equation is sometimes used in atmospheric general circulation models to infer the vertically integrated heating rate from latent heat release (Emanuel, 1994). A brief review of the water flux balance equation is presented first, followed with a more precise statement of problem.

Within a given column of the atmosphere, conservation of water substance requires that the flux of precipitation equals the upward vapour flux, plus the suface evaporation, minus the water storage in the cloud and possibly evaporation at cloud top (Holton, 1979, p. 342):

$$< P >=< q(z_b)\rho(z_b)w(z_b) > + < E > - < C > \tag{1}$$

where P is the precipitation rate (kg m^{-2} s^{-1}), q is the vapor mixing ratio (kg kg^{-1}), ρ is the density of air (kg m^{-3}), z_b is the top of moist boundary layer, w is vertical velocity (m s^{-1}), E is the surface evaporation rate (kg m^{-2} s^{-1}), and C is the rate of storage of water substance in the cloud and its immediate environment (kg m^{-2} s^{-1}). Angular brackets represent values averaged over the cross-section area. Since the storage and evaporation of water are relatively small for extensive layer clouds, the rainfall rate from stratiform clouds can be approximated by

$$< P >=< q(z_b) >< \rho(z_b)w(z_b) >=< q(z_b) > \int_o^{z_b} < -\rho\nabla \cdot \mathbf{V} > dz \tag{2}$$

where the mass continuity equation for deep convection $\partial(\rho w)/\partial z = -\rho\nabla \cdot \mathbf{V}$ has been used. It is difficult to obtain accurate convergence magnitudes derived from surface observations and balloon soundings. Instead of *in situ* measurements, remote sensing offers better opportunities for estimating the vertical profile of mass convergence. In many parts of the world, sensitive Doppler weather radars were recently installed to measure the radial wind throughout the lower portion of the tropopause (Crum and Alberty, 1993). When correcting for ground clutter and missing data, accurate divergence profiles can be obtained (Rabin and Zrnic, 1980; Rabin and Zawadzki, 1984).

Cloud models can be used to investigate physical mechanisms and interactions between dynamic, thermodynamic, and microphysical processes (Hill, 1974; Reuter and Yau, 1987). Models also offer great tools for sensitivity studies because model input variables can be changed in a controlled fashion. Intercomparing the results from sensitivity experiments reveals the dependence of an output parameter (such as rainfall) on input variables (Guan and Reuter, 1995). This is impossible from observations collected in field experiments, since in nature there are no "repetitions" of identical atmospheric conditions with only one parameter being changed.

The focus of this paper is to investigate the accuracy and sensitivity of estimating rainfall using the water flux balance relationship (2) by intercomparing with the results from a time-dependent non-hydrostatic cloud model. By changing the large-scale divergence profile, the initial thermodynamic profile becomes moist adiabatically adjusted within the lifted layer. Intercomparing the model experiments shows how the stratiform precipitation rate depends on the divergence profile. This allows for systematic testing of the water flux balance equation subjected to different conditions of moisture convergence.

2. Numerical model

The numerical cloud model has been developed by Steiner (1982), Reuter and Yau (1987), Guan and Reuter (1995), and Xin and Reuter (1996). It consists of the non-hydrostatic deep anelastic set of equations for conservation of momentum, air mass, heat and water substance. Perturbation pressure is computed from the diagnostic balance equation obtained from combining the momentum and continuity equations. Sub-grid scale exchange processes are parameterized using a first order closure scheme in which the eddy exchange coefficient depends on the local rate of deformation of the flow field, as well as on the local lapse rates of temperature and moisture (Hill, 1974). To keep computational requirements manageable, axial symmetry is assumed, i.e. the differential equations are written in cylindrical polar coordinates with the tangential gradients set to zero. This assumption is reasonable for modeling clouds in calm conditions (Guan and Reuter, 1995; Xin and Reuter, 1996).

Microphysical processes are modeled using a bulk water parameterization scheme. Three classes of water substance are considered: vapor, cloud water, and rainwater. Cloud water consists of droplets that move along with the surrounding air, whereas rainwater consists of drops that fall at a finite terminal velocity. The rainwater is assumed to have an exponential size distribution. Cloud water is converted to rain by auto-conversion, and collection by falling rain (Kessler, 1969). The threshold value for auto-conversion is a cloud water mixing ratio value of 1 g kg^{-1}. Details about condensation, fallout and evaporation of rain are given in Guan and Reuter (1995).

Omitting the ice phase microphysical processes in the model simulation requires some justifications. Previous studies indicated that including the ice microphysics is important for simulating precipitatation in squall lines (Tao and Simpson, 1987). Large consequences can accrue from the relatively small terminal velocity of snow. In the presence of vertical shear of the horizontal flow, snow falling from the upper regions of the convective line is transported large distances from their source before melting or reaching the surface. The associated negative buoyancy due to condensate drag and melting is thus far removed from the convective updrafts by large distances, with important dynamic consequences. Since the ambient flow in the the present model case does not exhibit mean vertical shear, no major dynamic differences would arise from the differences in terminal fall speeds of snow and rain. Also, the latent heat of fusion is only about 1/8 that of vaporization causing only minor thermal buoyancy differences (Reuter, 1987).

The large-scale convergent forcing is included in the model using a one-way open lateral boundary condition. The radial wind component at the boundary vary in height consistent with the density-weighted large-scale divergence profile. Assuming that the divergence profile does not vary in time implies that the radial wind components at the domain cylinder wall also remain constant with time. A detailed discussion of the motivation and implementation of the radial boundary condition is given in Xin and Reuter (1996). The top and bottom of the domain are rigid and free-slip boundaries. There is no transport of heat and moisture through the top and bottom boundaries, except for rainfall at the surface. The model equations are

solved numerically using a finite difference scheme on a staggered grid arrangement (Steiner, 1982). The computational domain has a depth of 12 km and a radius of 50 km. The vertical and radial grid spacing are 200 m and 400 m, respectively.

3. Control case simulation

To investigate the usefulness of the water flux balance relation for estimating area-averaged rainfall rates, we selected a case of widespread rainfall over central Alberta, Canada. Figure 1 shows the sounding sampled at 0000 UTC on 23 June, 1993 near Carvel (54.34°N, 114.09°W, 783 m above MSL). The airmass was saturated throughout a thick layer extending from 850 to 600 mb. It was stable for convective overturning with the exception of two shallow layers near 830 and 740 mb that were conditionally unstable. The lifted condensation level was at 885 mb with a temperature of 7°C.

The precipitation and wind field were monitored by the Doppler radar located at Carvel. The technical characteristics of this radar are a wavelength of 5.34 cm, an azimuthal beam width of 1.4°, a peak pulse power of 260 kwatt, a pulse length of 150 m, and a pulse repetition frequency of 1190 Hz. Doppler velocities were recorded in 220 gates, each 500 m long, spaced continously along the radar beams from three different elevation angles (0.5°, 1.5°and 3.5°). More information about the radar facility and data processing can be found in Reuter and Beaubien (1996).

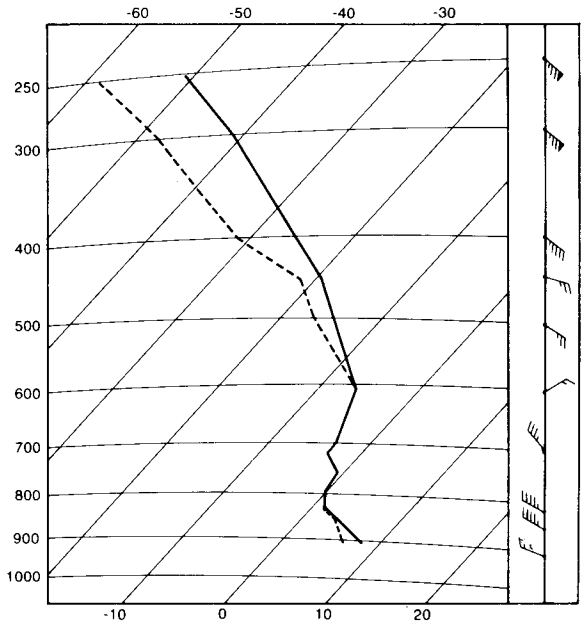

Fig. 1. Tephigram for sounding at Stony Plain (WSE) sampled at 0000 UTC 23 June 1993. The thick solid line depicts the temperature and the thick dashed line the dew-point.

The Doppler velocity measurements were analysed to retrieve the vertical profile of the area-averaged divergence, using the Extended Velocity Azimuth Display (EVAD) technique (Srivastava *et al.*, 1986; Matejka and Srivastava, 1991). In this method each radial velocity

measurement is approximated with a truncated harmonic series. The approximations are optimal in that they minimize a cost function consisting of weighted squares of deviations. Details on implementing the EVAD technique for velocity measurements sampled with the Carvel radar are presented by Xin (1996). Figure 2 shows the profile of area-averaged divergence derived from the EVAD analysis at 0030 UTC in the domain having a radius of 50 km. The flow was convergent in the layer from 0.6 to 2.4 km with a peak value of about 3×10^{-4} s^{-1}. The divergence profile for heights above 2.5 km could not be estimated accurately as the highest elevation angle was only 3.5°. It should be noted that the reflectivity pattern was sampled every 10 minutes with the highest elevation angle of 28°. The radar echo top defined by the 10 dBZ surface was around 6 km, suggesting that the large gradient in divergence between 2 and 2.5 km were not associated with echo top scattering. Also, the estimates of the errors in divergence derived from the EVAD method suggest that the accuracy of the divergence profile is about 10-15% in the layer $z = 0.5$ km to $z = 2.5$ km (Xin, 1996, chapter 2). Computations show that the profile of area-averaged divergence remained very similar throughout the period 0030 to 0400 UTC. The profile presented in Figure 2 was approximated with piece-wise linear segments to provide initial and boundary conditions for the model. To mimic the synoptic observations of a steady surface pressure, the net mass accumulation of air in the model domain was kept at zero by assuming a uniform divergence from 2.9 to 12 km (Xin, 1996).

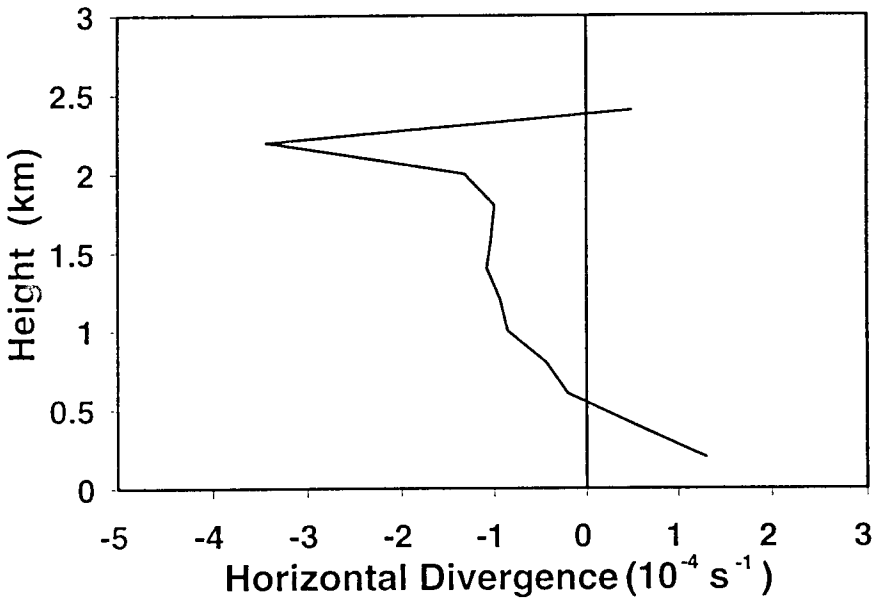

Fig. 2. Profile of divergence obtained from the Doppler velocity data with the EVAD analysis at 0030 UTC 23 June 1993.

Figure 3 shows the evolution of the peak updraft speed and the area-averaged surface rainfall for the control simulation. The peak updraft (defined as the maximum value over the domain) grows rapidly reaching a top speed of 3 m s^{-1} at about 70 min. After this initial spurt, the peak updraft subsides and remains close to 1.3 m s^{-1} for the next two hours. After three hours of simulation time, the peak upward motion becomes stronger again, oscillating between 1.5 and 3 m s^{-1}. The time history of accumulated area-averaged rainfall shows that rain first reaches the ground at about 50 min, accumulates to 5.6 mm at 2 h. The time history curves of peak updraft

and accumulated rainfall suggest that these first 2 h of variable rain rate should be considered as the "warming up" period. Within this time span, the model temperature profile becomes close to moist pseudoadiabatic. After the 2 h "warm-up" period, the rainfall accumulation increases almost linearly with time at a rate of 3.3 mm h^{-1}. The rainfall rate remains uniform for the remainder of the simulation.

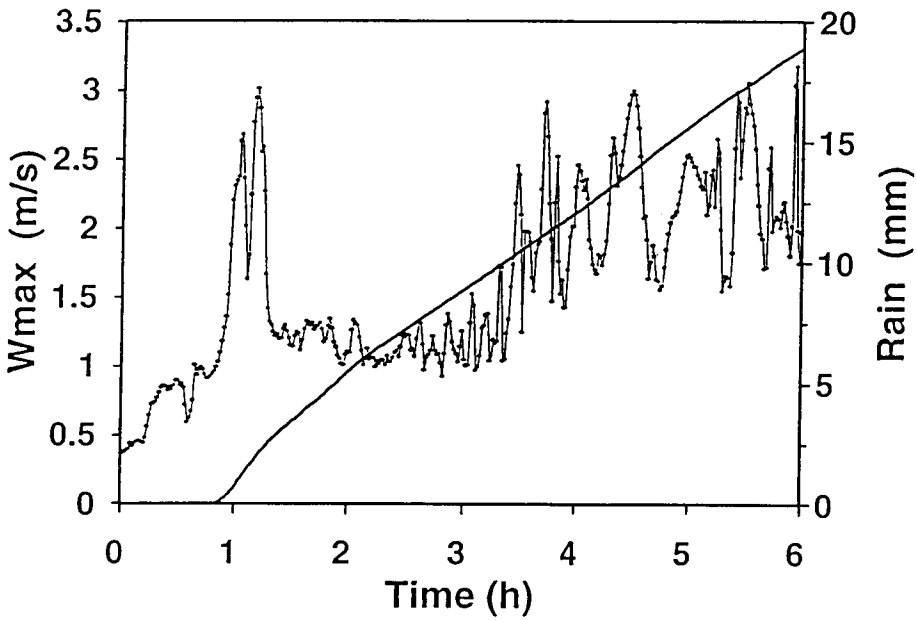

Fig. 3. Evolution of maximum vertical velocity w_{max} (thin line) and accumulated rain (thick line) for the control case simulation.

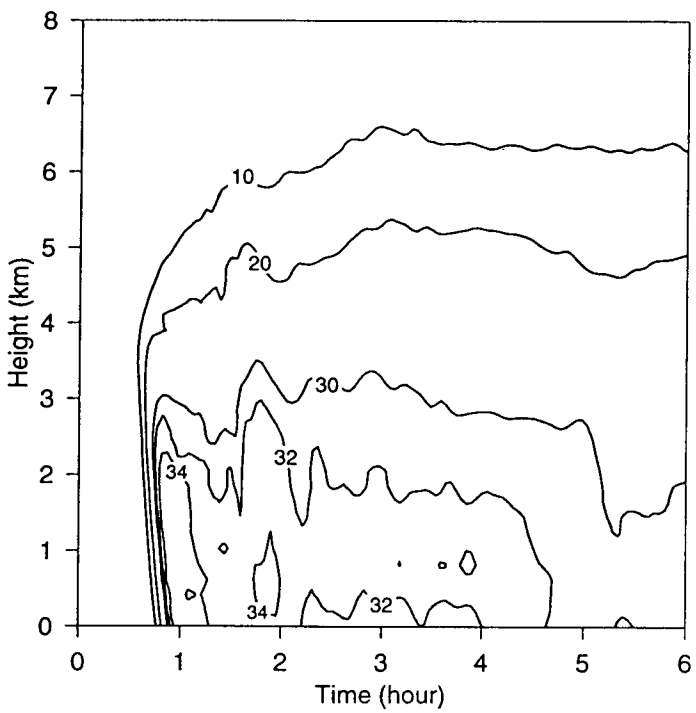

Fig. 4. Height-time pattern of area-averaged radar reflectivity contoured at 10, 20, 30, 32 and 34 dBZ for the control case simulation.

The cloud in the model is stratiform with only few short-lived cumulus cells embedded. The precipitation field shows little variability in the horizontal. Figure 4 shows the time-height pattern of the horizontally averaged radar reflectivity factor $< Z >$. From 45 to 80 min, $< Z >$ develops rapidly. The strongest cell forms about 500 m above ground with a peak value of 35 dBz . After 2 h, $< Z >$ weakens gradually aloft. The horizontally averaged reflectivity value of 10 dBZ remains close to 6 km from about 3 to 6 h. This agrees well with the observed 10 dBZ echo top height as recorded by the Carval radar (Fig. 5).

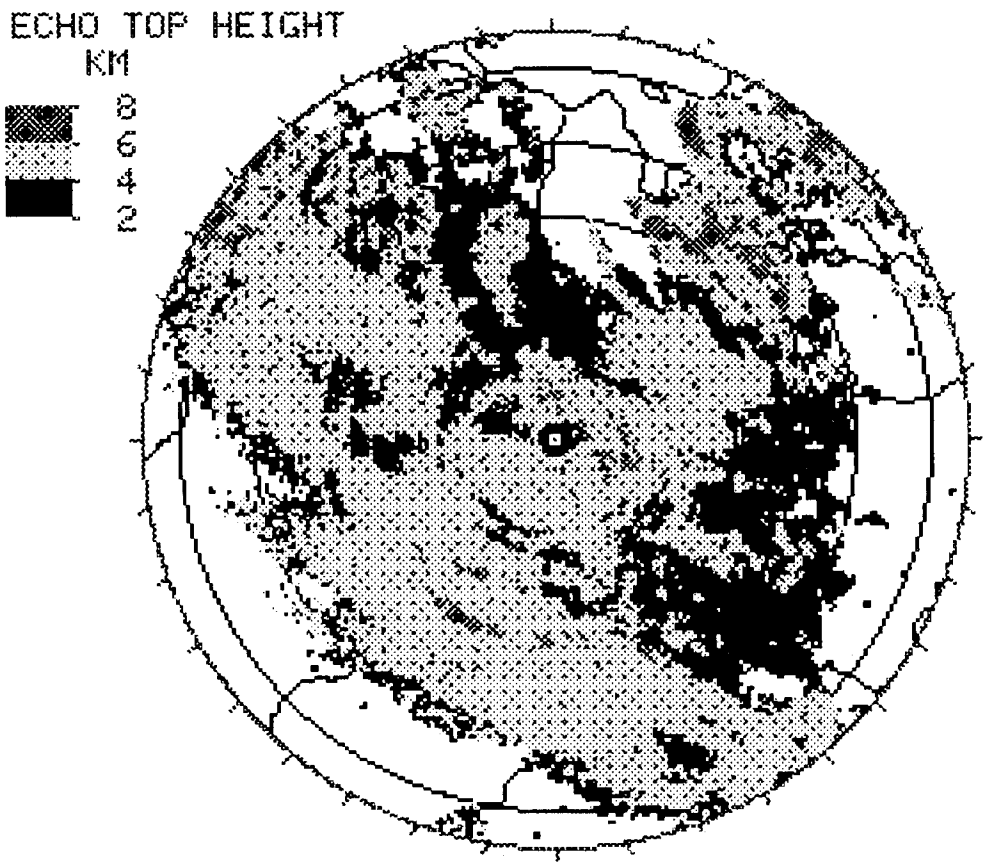

Fig. 5. Planar view of the radar echo top (10 dBZ contour) height in km recorded by the Carvel radar at 0030 UTC 23 June 1993.

The model rainfall was compared with surface observations to clarify whether the numerical model is suited to evaluate the water flux balance equation for estimating stratiform precipitation. The model rainfall rate averaged for the 4 h time period (from 2h to 6h) is compared with gauge observations (Table 1). The observed rainfall rates were obtained by averaging over the 0000 to 0600 UTC recording period. The comparison shows that the model overestimates the rainfall by about 18% to 27%, depending on which station is considered. For the mean overestimate of 22.5%, this is a 50% increase over the 15% error margin of rainfall observations.

Table 1. Comparison of cloud model rainfall rate with observations from three nearby synoptic stations.

Cloud model rainfall rate	3.3 mm h^{-1}
Stony Plain Station (53.33°N, 114.06°W)	2.7 mm h^{-1}
Edmonton Airport (53.19°N, 113.35°W)	2.8 mm h^{-1}
Edmonton City (53.30°N, 113.32°W)	2.6 mm h^{-1}

4. Evaluation of the water flux balance equation for estimating precipitation rates

In this section a comparison is made of the precipitation rate $< P >$ estimated from the water flux balance equation with that computed with the cloud model for various divergence profiles. All cases presented here are based on the same thermodynamic conditions (shown in Fig. 1) and an area-averaged divergence profile with its generic form sketched in Figure 6. Divergence extends from z_2 to z_4 with its maximum value (DIV_{max}) occurring at z_3. z_2 denotes the depth of the surface convergence layer that reaches its maximum convergence value (CON_{max}) at $z_1 = 0$ km. Eq. (2) can be combined with the continuity equation. For $z_b < z_2$, we have

$$< P >=< q(z_b)\rho(z_b)w(z_b) >=< q(z_b) > \int_o^{z_b} \{\rho\, CON_{max}(1 - z/z_2)\}dz$$

$$=< q(z_b) > \rho^* CON_{max}(z_b - 1/2 z_b^2 z_2^{-1}) \tag{3}$$

where ρ^* is the air density averaged for the layer $z = 0$ to $z = z_b$.

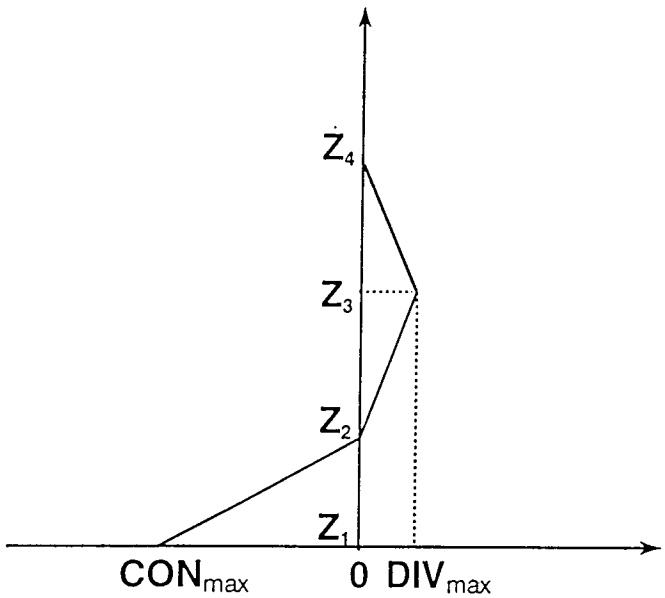

Fig. 6. Profile of divergence used in numerical cloud simulations M1 to M8, and D1 to D7. CON_{max} and DIV_{max} denote the maximum values of surface convergence and upper-level divergence.

Table 2 compares $< P >$ values from (3) with $< P >_{model}$ values using the cloud model. In all cases, the model simulations were made for six hours, and the listed $< P >_{model}$ values represent the four hourly time-averages from 2 to 6 h. The first 2 h were needed for "warm-up" to adjust the thermodynamic stratification and to develop rain. The eight experiments labelled M1 through M8 were designed to examine the dependence of the precipitation rate upon the magnitude of the maximum convergence (CON_{max}). The history of rainfall accumulation for these cases (shown in Fig. 7a) indicates that total rain amount increases roughly linearly with time. Rainfall increases with larger CON_{max}. Also, the onset of surface precipitation occurs sooner with the increase in the surface convergence. Evidently, an increase in surface convergence speeds up the rain formation. The curves of precipitation rate versus CON_{max} are plotted in Figure 7b. The model precipitation rates $< P >_{model}$ are higher than the $< P >$ values from (2), suggesting that the simple water flux relationship underestimates the precipitation rates by about 25%.

Table 2. Comparison of rainfall rates from the water flux balance equation $< P >$ and from the numerical cloud model $< P >_{model}$ for different values of maximum surface convergence (CON_{max}) and convergence depth (z_2).

Case	CON_{max} ($10^{-4}s^{-1}$)	depth z_2 (km)	<P> (mm h^{-1})	$<P>_{model}$ (mm h^{-1})
M1	0.4	3.0	0.90	1.45
M2	0.6	3.0	1.34	1.84
M3	0.8	3.0	1.79	2.31
M4	1.0	3.0	2.23	2.63
M5	1.2	3.0	2.77	2.97
M6	1.4	3.0	3.12	3.42
M7	1.6	3.0	3.57	3.96
M8	1.8	3.0	4.01	4.82
D1	1.0	1.0	0.99	1.31
D2	1.0	1.5	1.48	1.77
D3	1.0	2.0	1.86	2.11
D4	1.0	2.5	2.08	2.70
D5	1.0	3.0	2.23	2.70
D6	1.0	3.5	2.33	2.97
D7	1.0	4.0	2.41	3.29

Table 2 also shows sensitivity results for the depth of the convergent layer. Cases D1 to D7 have the same maximum convergence value, CON_{max}, but their convergence depths z_2 differ

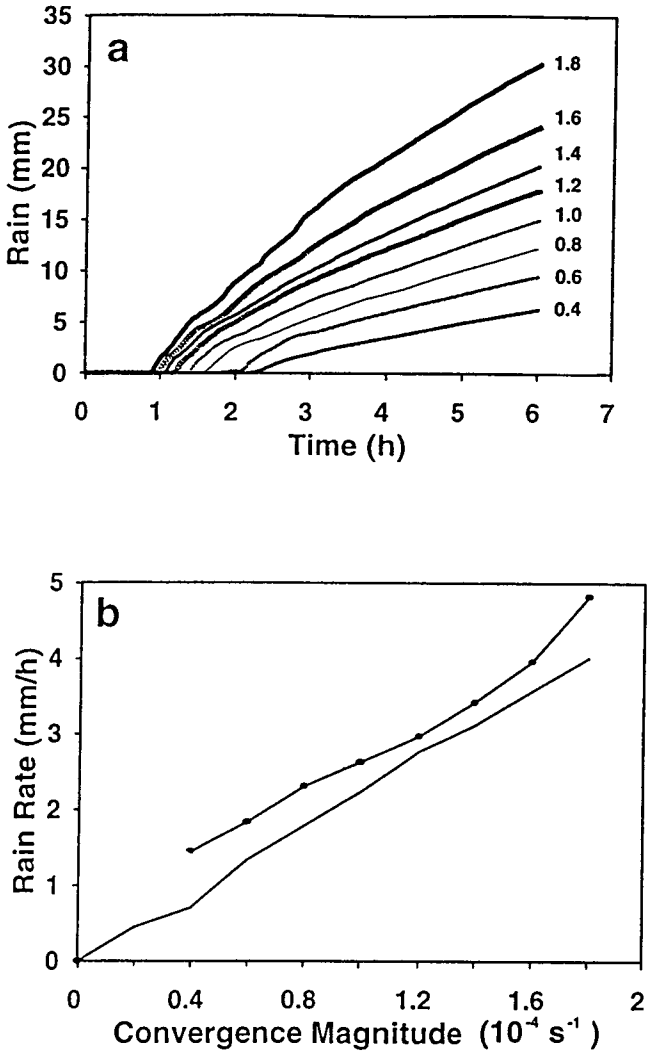

Fig. 7 (a) Area-averaged accumulated rainfall plotted versus time for simulations M1 through M8. The curve labels list the magnitude of maximum convergence (CON_{max}) in units of 10^{-4} s^{-1}. (b) Area-averaged rainfall rate plotted versus surface convergence magnitude (CON_{max}) The solid line shows the water flux balance relationship, while the line with the data points shows the cloud model results.

from 1 to 4 km. Figure 8a shows the evolution of the rainfall accumulation. As the convergence depth is increased, more rain accumulates at the ground. Also, the onset of rainfall is more rapid. The rainfall curves for the convergence depths of 2.5 km and 3 km are rather interesting: The similar slopes of the curves indicate similar rainfall rates. This similarity is related to the sounding profile which shows a very stable layer from 2.5 to 3 km. The model rainfall curves, however, differ in that the 3 km convergence depth yields surface rainfall at an earlier stage. Comparing the $< P >$ and $< P >_{model}$ values (in Fig. 8b) suggests that the water flux balance equation underestimates the rainfall, particularly when deeper convergence layers exist. However, $< P >$ and $< P >_{model}$ curves agree that deeper convergence results in larger rainfall rates when CON_{max} remains unchanged.

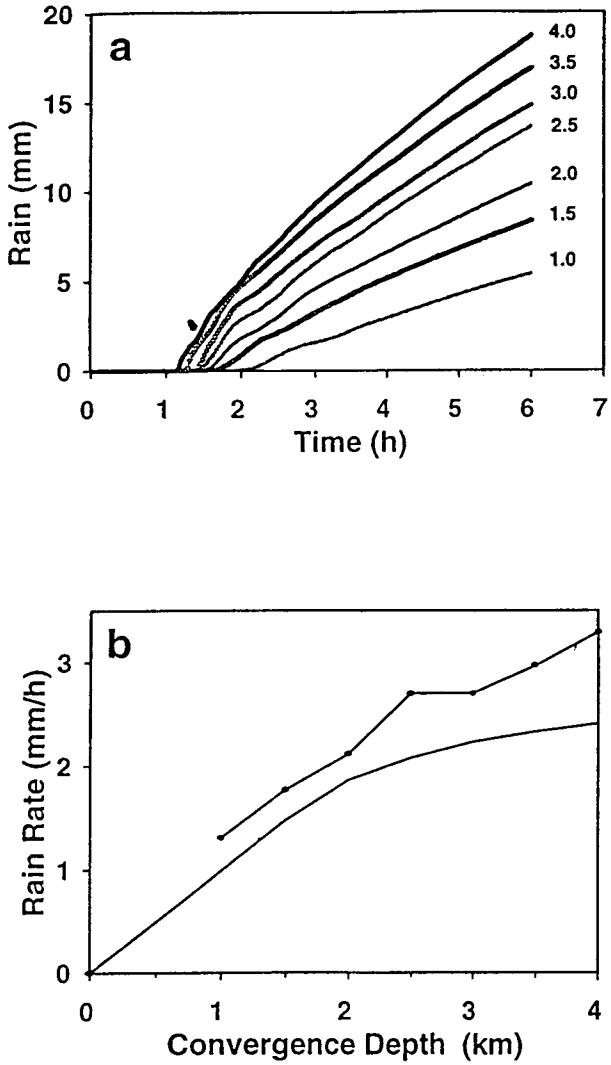

Fig. 8. (a) Area-averaged accumulated rainfall plotted versus time for simulations D1 through D7. The curve labels list the depth of the surface convergence layer in units of km. (b) Area-averaged rainfall rate plotted versus convergence depth. The solid line shows the water flux balance relationship, while the line with the data points shows the cloud model results.

The next set of model experiments (labelled UD1 to UD4) has been designed to examine the sensitivity of rainfall to the distribution of the upper level divergence. Figure 9 shows the divergence profiles used to specify the initial and boundary conditions for experiments labeled UD1 to UD4. All four experiments have the same magnitude and depth of convergence ($\mathrm{CON}_{max} = 10^{-4}$ s^{-1} and $z_2 = 1$ km). Furthermore, in all cases the shape of the divergence profile is a symmetric "V" with the top of the divergence set at the height of 9 km. However, experiments differ in the depth of their divergence layers. The maximum divergence value is chosen such that the total (density-weighted) height-integrated divergence is zero: That is, the divergence aloft balances the low-level density-weighted convergence to assure strict conservation of air mass within the

model domain. In all four cases UD1 to UD4, surface rainfall starts at the same time, just after 2 hours (Fig. 10a). Thus the onset of rainfall is not affected by the vertical distribution of the upper-level divergence. However, the modelled rainfall amount is slightly sensitive to the divergence profile aloft. When the divergence is spread out over a deep layer from 1 to 9 km (case UD1) the rainfall is weaker compared to the case when all the divergence occurs in the more shallow layer from 4 to 9 km (case UD4). The intermediate cases yield rainfall amounts that lie between these extremes. However, for all cases, the difference in total rainfall amount is fairly small, varying by less than 20% from 6 mm. Figure 10b shows the same results in terms of average rainfall rates plotted versus divergence maximum. The area-averaged rainfall rate becomes larger when the magnitude of the divergence maximum is increased (associated with a decrease in the depth of the divergent flow aloft). The model rainfall rates vary between 1.32 and 1.56 mm h^{-1}.

An obvious shortcoming of the water flux balance equation $< P >=< q(z_b)\rho(z_b)w(z_b) >$ is that the precipitation rate is independent of the divergence profile above the level of moist air z_b. This contradicts the cloud model results (for cases UD1 to UD4) that show that the vertical distribution of the upper-level divergence has a certain impact on the rainfall rates even when the total vertically integrated divergence remains unchanged. We did not investigate cases where the total upper-level divergence is increased since this would result in a decrease in mass and cause a drop in surface pressure. Once the surface pressure falls, the low-level convergence field would likely be affected causing other dynamic feedbacks that would make direct model-model intercomparisons problematic. Suffice to note here is that the simple water flux balance relation misses the effects of upper-level divergence which can influence the surface rainfall in some conditions.

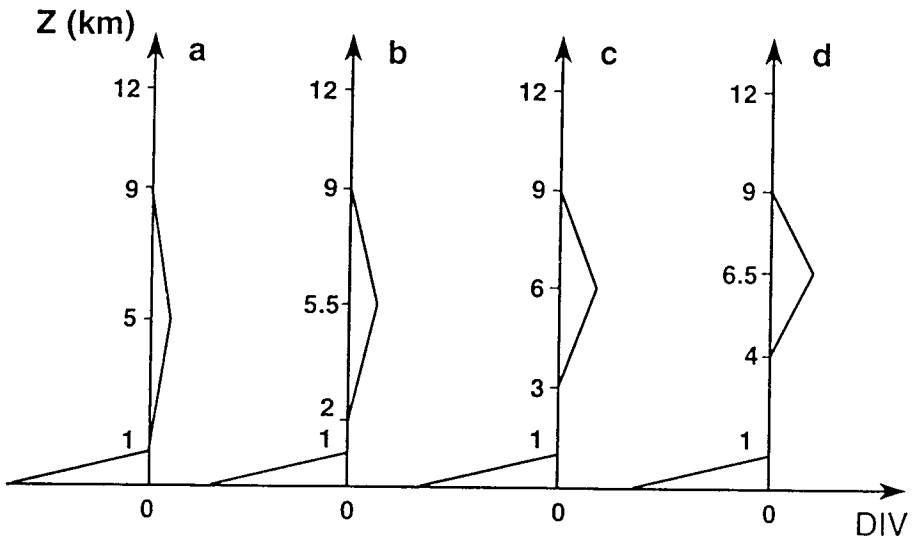

Fig. 9. Vertical profile of divergence used in cloud simulations (a) UD1, (b) UD2, (c) UD3, and (d) UD4.

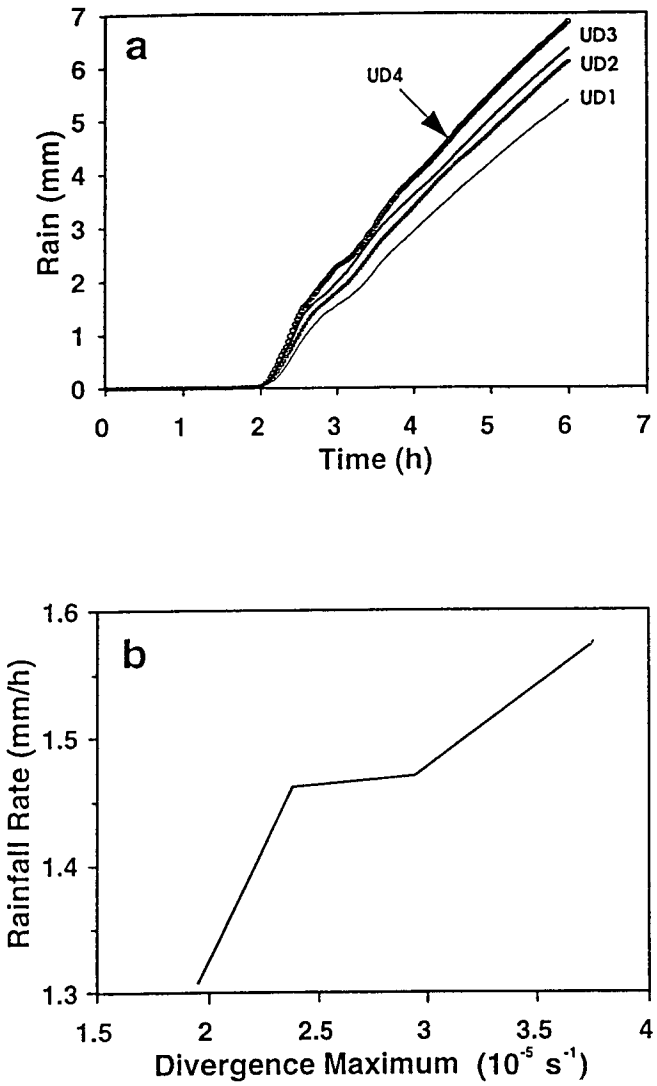

Fig. 10. (a) Area-averaged accumulated rainfall plotted versus time for simulations UD1 through UD4. (b) Area-averaged rainfall rate plotted versus maximum divergence value based on cloud simulation results.

5. Discussion and conclusion

The water flux balance relation equates the upward water vapour flux with the downward flux of precipitation, thereby providing a simple diagnostic estimate for the area-averaged precipitation rate. In its simplest setting, the precipitation rate equals the product of updraft speed, air density and vapour mixing ratio values that are horizontally averaged at the top of the moist surface layer (z_b). This diagnostic relationship is only appropriate for stratiform rain since its key assumption is that of steady-state balance. The precipitation estimate can be sensitive to z_b when the moist boundary layer is not clearly marked. Often, however, the low-level vapour content profile is rather uniform due to evaporating rain below cloud base and turbulent mixing. This makes the particular choice of z_b rather unimportant.

To examine the accuracy of the water flux balance equation for estimating stratiform rainfall rates, they were compared against results computed with a numerical cloud model. We are aware that the cloud simulations presented here have shortcomings in that they neglect ambient wind shear and ice phase processes. Averaging the rainfall rate over the entire horizontal area and over a time span of a few hours should smooth many of the details that are associated with the shear and ice microphysics. Since this model has been found to mimic nature realistically for a particular stratiform rainfall occurrence in central Alberta of Canada, it should be a reliable tool for making sensitivity experiments when using the same thermodynamic conditions.

Compared against the cloud model, the water flux balance equation tends to underestimate the area-averaged precipitation rates by about 25%. The water flux balance estimates agree with the cloud model ones in that the rainfall increases when the magnitude of the surface convergence becomes larger. Also, the water flux balance yields a strictly linear increase, while the cloud model results suggest a non-linear increase. The water flux balance relation and the cloud model agree that the precipitation rate increases monotonically when the depth of convergent flow is increased. However, compared to the model, the water flux balance equation underestimates the increase in rainfall when the convergence layer becomes very deep. The model results show the effect of upper-level divergence on the intensity of surface rainfall. This contribution is not incorporated in the water flux equation which is a significant weakness of this simple equation.

Acknowledgements

This research was supported by Environment Canada and the Natural Science and Engineering Research Council of Canada. We acknowledge the thoughtful comments by a reviewer that helped to improve the manuscript.

REFERENCES

Crook, N. A., and M. W. Moncrieff, 1988. The effect of large-scale convergence on the generation and maintenance of deep moist convection. *J. Atmos. Sci.*, **45**, 3606-3624.

Crum, T. D., and R. L. Alberty, 1993. The WSR-88D and the WS-88D operational support facility. *Bull. Amer. Meteor. Soc.*, **74**, 1669-1687.

Emanuel, K. A., 1994. Atmospheric Convection. Oxford University Press, New York, 580 pp.

Guan, S., and G. W. Reuter, 1995. Numerical simulation of a rain shower affected by waste energy released from a cooling tower complex in a calm environment. *J. Appl. Meteor.*, **34**, 131-142.

Hill, G. E., 1974. Factors controlling the size and spacing of cumulus clouds as revealed by numerical experiments. *J. Atmos. Sci.*, **31**, 646-673.

Holton, J. R., 1979. An introduction to dynamic meteorology. 2nd edition. Academic Press. New York, 391 pp.

Hudson, H. R., 1971. On the relationship between horizontal moisture convergence and convective cloud formation. *J. Appl. Meteor.*, **10**, 755-762.

Kessler, E., 1969. On the Distribution and Continuity of Water Substance in Atmospheric Circulations. Meteor. Monogr., No. 32, *Amer. Meteor. Soc.*, 84 pp.

Lipps, F. B., and R. S. Hemler, 1986. Numerical simulation of deep tropical convection associated with large-scale convergence. *J. Atmos. Sci.*, **43**, 1796-1816.

Maddox, R. A., 1983. Large-scale meteorological conditions associated with midlatitude, mesoscale convective complexes. *Mon. Wea. Rev.*, **111**, 1475-1493.

Matejka, T. J., and R. C. Srivastava, 1991. An improved version of the extended velocity-azimuth display analysis of single-Doppler radar data. *J. Atmos. Oceanic Technol.*, **8**, 453-466.

McBride, J. L., and W. M. Gray, 1980. Mass divergence in tropical weather system. I: Diurnal variations. *Quart. J. Roy. Meteor. Soc.*, **106**, 501-516.

Ogura, Y., M.-T. Liou, J. Russell, and S. T. Soong, 1979. On the formation of organized convective systems observed over the eastern Atlantic. *Mon. Wea. Rev.*, **107**, 426-441.

Rabin, R. M, and D. S. Zrnic, 1980. Subsynoptic-scale vertical wind revealed by dual Doppler radar and VAD analysis. *J. Atmos. Sci.*, **37**, 644-654.

Rabin, R. M., and I. Zawadzki, 1984. On the single Doppler measurements of divergence in clear air. *J. Atmos. Oceanic Technol.*, **1**, 50-57.

Reuter, G. W., 1987. Penetrative downdrafts in mixed-phase clouds. *S. Afr. J. Phys.*, **10**, 139-145.

Reuter, G. W., and M. K. Yau, 1987. Mixing mechanisms in cumulus congestus clouds. Part II: Numerical simulations. *J. Atmos. Sci.*, **44**, 798-827.

Reuter, G. W., and R. Beaubien, 1996. Radar observations of snow formation in a warm prefrontal snow band. *Atmos.-Ocean*, **34**, 605-626.

Soong, S.-T., and Y. Ogura, 1973. Response of trade wind cumuli to large-scale processes. *J. Atmos. Sci.*, **37**, 2035-2050.

Srivastava, R. C., T. J. Matejka, and T. J. Lorello, 1986. Doppler radar study of the trailing anvil region associated with a squall line. *J. Atmos. Sci.*, **43**, 356-377.

Steiner, J. T., 1982. An axially symmetric cloud model: Development and simulations. Storm Weather Group, Scientific Report. MW-94, McGill University, 55 pp.

Tao, W.-K., and J. Simpson, 1989. Modeling study of a tropical squall-type convective line. *J. Atmos. Sci.*, **46**, 177-202.

Tollerud, E. I., and S. K. Esbensen, 1985. A composite life cycle of nonsquall mesoscale convective systems over the tropical ocean. Part I: Kinematic fields. *J. Atmos. Sci.*, **42**, 823-837.

Ulanski, S. L., and M. Garstang, 1978. The role of surface divergence and vorticity in the life cycle of convective rainfall. Part I: Observations and analysis. *J. Atmos. Sci.*, **35**, 1047 1062.

Wilson, J. W., and W. E. Schreiber, 1986. Initiation of convective storms at radar-observed boundary-layer convergence lines. *Mon. Wea. Rev.*, **114**, 2516-2536.

Xin, L., 1996. Effects of mesoscale convergence on convective and stratiform rainfall: Radar observations and numerical simulations. Ph. D. thesis, University of Alberta, Edmonton, 178 pp.

Xin, L., and G. W. Reuter, 1996. Numerical simulation of the effects of mesoscale convergence on convective rain showers. *Mon. Wea. Rev.*, **124**, 2828-2842.